Anomalous spin-orbit fluctuating dynamics using enhanced Raman shift of magnetic resonance force microscopy perovskite multi-films

R. REN[*], YIJING REN, ZHENG WU, DANAN REN, ZHONGXIA ZHAO, JIN XU, HAODI XU, XUAN LI, LIN LIU, LEI BAI
Department of optics, Xi'an Jiao Tong University, Xian 710054, China

Raman active phonon in orthorhombic perovskite $La_{0.7}Sr_{0.3}MnO$ films and ZnO/LSMO multi-films were focused by measuring Raman spectra of 325 nm and 512nm laser in scattering configurations. The results show that the spin-orbit is caused by anomalies tilt of MnO_6 octahedron. The transfer of $d_{x^2-y^2}$ orbits dynamics is in the background of the ferro-orbital order state of crystal stabilized $d_{3z^2-r^2}$ orbit effect. The kinetic energy gain achieved by the orbital competition, strong crystal field and charge order of energy band splitting. The LSMO/ZnO junction exhibits excellent junction behavior over the temperature range of 77–300 K.

1. Introduction

One foundational issue in the physics of perovskite is the role of spin-orbital degrees of freedom as well as the state of the orbit subsysytem at different doping levels. LaSrMnO₃ colossal magnetoresistance oxides are the most promising materials of the orbital degrees of freedom as well as orbital subsystem at different doping level and structure in studying the complex phase dynamics. [1] The doped manganese oxides $La_{0.7}Sr_{0.3}MnO_3$ (LSMO) displays competition coupling of spins, charge, orbit, and lattice order because of its pronounced two-dimensional structural and electronic characteristics. With reducing temperature the ferromagnetic samples exhibit cooperative Jahn-Teller distortion. [2,3] Further cooling a transition from a paramagnetic insulating (PI) to a ferromagnetic (FM) state was occurred at Tc where the resistitivity begin to reduce. Also, ZnO is a most popular semiconductor material with a wide band gap (3.37 ev) and large exciton binding energy (60 mev). [4,5,6] The low dimensional nano-heter-junction of LSMO changes the orbital and spin dynamics.

LSMO crystallizes in the perovskite type tetragonal structure R3C, with O(1) in plane and O(2) apical oxygen sites as some high-Tc cuprates. In LSMO, Raman scattering is sensitive for the active phonon modes and stretching modes of both local and spatially coherent structural changes. The MnO_2 magnetic layers are stacked along the c axis and separated by LaO_2, SrO_2 plane. LSMO is known to be a interesting structure to research the ferr-orbital ordering of $d_{3Z^2-r^2}$ orbitals and a C-type antiferromagnetic (AF) spin ordering below TN, which charge and orbital ordered phase caused by electron-phonons dynamics [7,8,9,10].

Ferroelectric ZnO contains transition metal ions with unpaired d electrons. The heterojunction $ZnO/La_{0.7}Sr_{0.3}MnO_{3+\sigma}$ nanostructure is good candidate for fabrication of nanometer-sized optoelectronic devices. It is expected that structural changes and spin-orbital magnetic order will influence the electron-phonon spectra. The doped strontium $La_{0.7}Sr_{0.3}MnO_{3+\sigma}$ and ZnO junctions with carrier transfer exhibit photoinduced resistance and colossal magnetoresistance (CMR) effect [1].

So far, Zheng, RK focused on effects of the strain induced by ferroelectric poling of $LaMnO_3$ grown on $Pb(Mg_{1/3}Nb_{2/3})O_3$-$PbTiO_3$ substrates, and explored the strong coupling of charge carriers to JT distortion for understanding the effects of the substrate-induced strain in manganite thin films. [12] The transport behavior accompanying domain switching was reported in $La_{0.1}Bi_{0.9}FeO_3/La_{0.7}Sr_{0.3}MnO_3$. [15] Arindam used nonequilibrium magnetotransport spectroscopy to explore spin polarization at low temperature and a strong sensitivity of such polarization to magnetic fields. [13] Those groups have reported the growth of two dimensional heterojunction nanostructures using different methods. The lower dimensionality changes the orbital and spin coupled dynamics, and either related to more pronounced fluctuations or raise orbital degeneracies. [2] Although other Raman spectra have been reported, there are few

perovskites spectra information on the lattice dyanamics in heterojunction films as well as to analyze more specific aspects of phonon-electrons interactions.

The LSMO has a tetragonal structure structure, (*I4/mmm*) space group, with O(1) in-plane and O(2) apical oxygen sites. The LaO_2 and SrO_2 planes are stacked along a-b axis and separated by the MnO_2 planes as the result of a ferromagnetic-orbital ordering of orbital d_{3z2-r2} and C-type antiferromagnetic (AF) spin ordering below T=117-127k. The presence ZnO of the *d* electrons can result in a relatively small gap and give rise to a concentration of charged impurities and defects. [14] The question is whether the spin-orbital degrees of freedom are a relevant parameter to describe the properties of ZnO/$La_{0.7}Sr_{0.3}MnO_3$ characteristics.

In this letters, we reported Raman scattering studies of ZnO/$La_{0.7}Sr_{0.3}MnO_{3+\sigma}$/LaAlO heterojunction with different nano-thickness structure to investigate spin-orbital dynamics of phase transition from insulator to metal. We prepared multi-crystal LSMO/ZnO to introduce MR and carrier injection. A temperature dependence of positive magnetoresistance was observed in this junction that has some special properties of ferromagnetic semiconductor, [8,9] multilevel resistive switching, [10] positive colossal magnetoresistance, [11, 12] colossal electroresistance, [13] manganite tunnel junctions [14], high magnetic sensitivity [23] and ultraviolet fast-response [23].

2. Model and experiment

The fabricated strontium perovskites $La_{0.7}Sr_{0.3}MnO_{3+\sigma}$ and ZnO thin films were grown on LaAlO substrate by pulse laser abation method. The LSMO thin film about 220nm (estimated by SpecEI-2000-VIS ellipsometer) was deposited on $LaAlO_3$ (100) with the substrate kept at 800°C and oxygen pressure 10 Pa. The $La_{0.7}Sr_{0.3}MnO_{3+\sigma}$ doped oxygen displayed difference proportion of Mn^{3+} and Mn^{4+}. The ZnO film bout 75nm was deposit masked on $La_{0.7}Sr_{0.3}MnO_{3+\sigma}$ (100). At respective temperatures, neutron and X-ray studies show a superstructure interpreted in terns of long-range charge order. The structure of the target and the orientation of the deposited film were studied by XRD (Bruker D8 Advance XRD, 40KV, 40mA, smallest angular step 0.0001^0).

When σ increases 0.073-0.120, a distorted orthorhombic O' phase changes to a pseudocubic one (σ) then transits to a rhombohedral one. The systematic distortions of the MnO_6 octahedra was lowered by continuously the Mn^{4+}/Mn^{3+} ratio. The ZnO/ LSMO structure was characterized by x-ray diffraction pattern at 180k, 220k, 250k shown in Fig. 1(a)(b)(c). Raman spectra of films were measured in a quasiback scattering with the excitation line λ =514nm of Ar laser, 325nm of solid-state laser with the power of 8mW and were collected by Raman spectrometer (HR800,HORZBA,Jobin Yvon) and a nitrogen cooled charge-coupled device detector. The grain refinements showed LSMO sample crystal belong to the hexagonal perovskite structures (space group:R-3C) with O(1) in-plane and O(2) apical oxygen sites.

3. Results and discussion

The XRD image indicated that the $La_{0.7}Sr_{0.3}MnO_{3+\sigma}$ (100) and (200) diffraction peaks occurred at 2θ =23^0 and 2θ =47^0, while the ZnO (100) (002) (101) (102) (110) (103) (200) diffraction peak occured at 2θ =31.59^0, 2θ =34.37^0, 2θ =36.09^0, 2θ =47.3^0, 2θ =56.4^0, 2θ =62.78^0 and 2θ =66.15^0. Besides the spectrum peak showed orientation of LSMO crystal plane, the diffraction peak of LAO (100), (200) substrate appear at 2θ =23^0 and 2θ =47^0. This identified LSMO film which was identical in the crystal plane orientation (100) with the LAO substrate had the multi-crystal structure. The diffraction peak of $La_{0.7}Sr_{0.3}MnO_3$/ZnO was matched with the LAO substrate (lattice constant 0.38769 nm) when the lattice constant was 0.386 and 0.379nm respectively. The results indicated that the $La_{0.7}Sr_{0.3}MnO_3$ and ZnO thin films had better epitaxial characters respectively. The ZnO film is 2θ =34^0 for the (002) orientation with the structure of a hexagonal wurtzite.

Raman spectra polarizations are shown in Fig. 2. For LSMO the space group R3C, the factor group analysis yields four Raman-active phonon modes: The Mn^{3+}-O-Mn^{4+} and $La(Sr)O_2$ extending modes have stretched along the c axis with A_{1g} symmetry. We measured the O and La(Sr) vibrations with shifting along the a and b axis with E_g symmetry.

For LaSrMnO and ZnO Raman shift, the factor group analysis displays four Raman active phonon modes: 150, 220, 490 and 620cm^{-1}. The group analysis yields four Raman active phonon modes: Mn-O(2) and (La,Sr)-O(2) stretching modes have displacement along the c axis with A_{1g} symmetry and O(2) and (La,Sr) vibrations with displacements along the a and b axes with Eg symmetry. A large and continuous softening of Mn-O bond stretching modes below the Curie temperature and an broadened, loose multiphonon feature indicate a fluctuating orbital state in FMI sample. We can find LaSrMnO E (TO_1) soft mode in the first brillouin zone. LaSrMnO Raman spectrum contains ten kinds of typical single mode E (TO_1), E (LO_1), A_1 (TO_1) E (TO_2), B_1+E, A_1 (TO_2), E (LO_2), E (two-to-three), A_1 (two-to-three) and A_1 (LO_3). If the LSMO has tiny distortion of crystal lattice, the size of Mn^{4+} and Mn^{3+} atom corresponds to Mn-O chain expansion. The stretching leads to rotating, tilt of octahedral and vibration of heavy rare metals. The Mn^{3+} became Mn^{4+} with absorption of oxygen. These forbidden peaks are weak in intensity but show a well defined symmetry. We can find the phonon modes dependence in frequencies at 192,210,325,430,649cm^{-1}, which rules out impurities and defects as a possible origin.
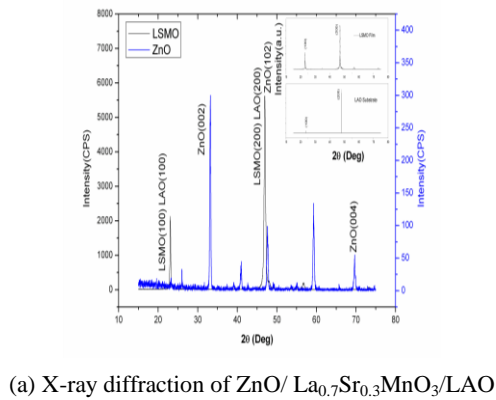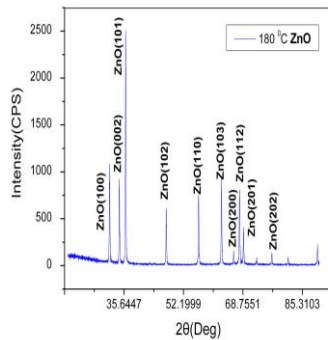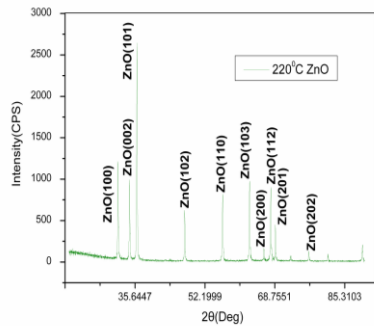
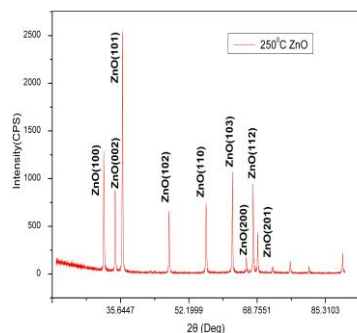(a) X-ray diffraction of ZnO/ $La_{0.7}Sr_{0.3}MnO_3$/LAO

(b) X-ray diffraction of ZnO film at 180^0C.

(c) X-ray diffraction of ZnO film at 220^0C.

(d)   X-ray diffraction of ZnO film at 250^0C

Fig. 1(a)(b)(c)(d). X-ray diffraction pattern of ZnO/ $La_{0.7}Sr_{0.3}MnO_3$/LAO heterostructure. The insets shows the (100) and (200) peaks of the LSMO film and LAO substrate.X-ray diffraction of   ZnO heterostructure at 180^0C, 220^0C,250^0C.
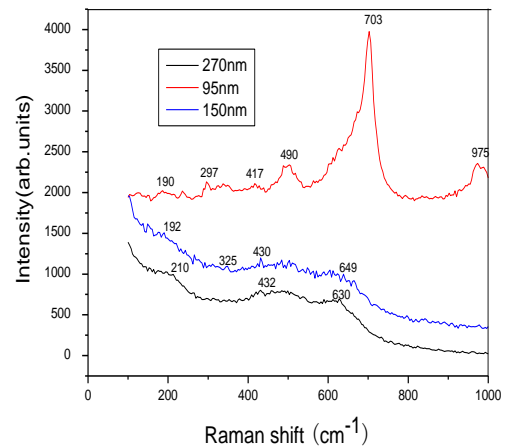

Fig. 2. Raman scattering spectrum of LSMO film with wavelength of 514 nm laser. The thickness dependence on Raman scattering in polarization in LSMO. The markert dots   are a guide for the eyes for the evolution of Mn-O(1) phonon modes.

We start to the distortion of MnO_6 octahedron. The different spectrum peak is shifted with film thickness in Fig. 2. The peak at 490 cm^{-1} moved to low frequency direction, while the peak at 703 cm^{-1} shifted to high frequency. The Raman peaks at 703 cm^{-1} corresponds to the ab in-plane phonon mode. The peaks at 490 cm^{-1} corresponds to ab vertical plane of the bended phonon modes. The Sr^{2+} doping amount on different level is not only changed the bond angle and bond length of Mn-O-Mn, but also make the octahedron of MnO_6 distorted. The experiment displayed the oxygen goes into the LSMO lattice after nealing. The Mn^{3+} ion became to Mn^{4+} ion. The Mn^{3+} ion radius (0.07 nm) is more than Mn^{4+} (0.05 nm) ionic radius, which leads to shrinkage 0.04 nm in the lattice constant.

The experiment also displays the respective spectrum in four polarization, where a and b correspond to the polarization of incident or scattering light along the MnO(1) direction. We observed the LSMO plane polarization. These scattering peaks are formed by $A_{1g}+B_{1g}$, $A_{2g}+B_{2g}$, $B_{1g}+A_{2g}$, and $A_{1g}+B_{2g}$ symmetries, respectively. The huge-magnetoresistance ferr-electricity phase transition of mulitilayers heterjunction could be revealed by lattice vibrated mode of Lamar spectra as well as the spin polarization and dielectric properties information could be explored.

The figure shows the Raman scattering spectra of LSMO films with wavelength of 325 nm He-Cd laser. The scattering peaks of *LSMO* 95 nm film appear at 320 cm^{-1},480 cm^{-1},602 cm^{-1}, and 675 cm^{-1},542 cm^{-1}. The characteristic peaks near at 310 cm^{-1}is for the tilt vibration of MnO6 octahedral. It corresponds to the bond angle changes of Mn^{3+}-O-Mn^{4+}. The frequencies of 602, 570, and 580 cm^{-1} corresponds to orthogonal cubic phase, which is MnO_6 octahedral stretching with the symmetric

and antisymmetric vibration characteristic peaks. The scattering peaks at 570 cm^{-1} 580 cm^{-1} is Jahn Teller transition phase. The characteristic peak at frequency 702 cm^{-1} exhibits the direction of rhombus antisymmetric stretching mode. We observe weak A_{1g} phonon signals at the frequencies of 203 cm^{-1} and 310 cm^{-1} as in (cc) polarization. The octahedral tilt MnO_6 vibration peak is at 310 cm^{-1} which is a A_{1g} symmetry. The vibration phonon mode of oxygen atoms is a 'soft mode'. The Raman shift corresponds to tilt of MnO_6 octahedral.

We observed lattice structure and physical properties ZnO/ LSMO as a result of changes of crystal field, temperature, strain, and interface roughness. The activated peaks are pronounced in the middle frequency range of 190-490 cm^{-1}. We focus on harmonic oscillator model of lattice vibration. The LSMO film thickness increases, while the axis of rhombohedral phase gradually enhances. The c axis gradually decreases due to an axis rise up and c axis left down. The adjacent angles between MnO_6 octahedron were improved. Because the Mn-O(1) distance is a little shorter than Mn-O(2), the Mn-O(1) frequencies are higher than 400 cm^{-1} of Mn-O(2) mode. With increasing characteristic vibrational energy A_{1g}, the A_{1g} peak shift largely. From 95 nm to bulk, A_{1g} characteristic peak move to the higher frequency direction that those wave number has maximal shift. The anti-symmetric stretching mode E_g is from 675 cm^{-1} to 649 cm^{-1}. Because the a axis increase, the vibration energy of MnO_6 octahedral stretching decreases, which low frequencies corresponds to MnO spinic and rare element vibration. The former modes are similar to excitations of LSMO with splitting that set in with the charge-exchange type and orbital order. The out plane d_{3z}^2-r^2 orbital character in LSMO is enhanced at low temperature which due to an increase of the tetragonal distortion of MnO_6 octahedron. The middle frequencies correspond to octahedral MnO_6 tilting. The high frequencies correspond to MnO stretching. In addition, Raman scattering peak of LSMO, as the film thickness reduce from bulk to 270-95 nm thickness. The peaks near 310 cm^{-1} move to low wave number and low frequency.

For excited Ar^+ laser, Jahn Teller at 703 cm^{-1} emerged in the series of distorted peak at 630, 640 and 703 cm^{-1}. The characteristic peak at 703 cm^{-1} with 325 nm excited laser is rhombohedral phase with no Jahn Teller distorted peak. The film performs the coexistence of two phase structures. There are rhombohedral phase and Jahn Teller distorted peak at 703 and 640 cm^{-1}. The distortion of octahedra $LaSrMnO_3$ lead to spin-orbit couple to crystal lattice, as the result of lattice and spin-orbit coupling between upper t_{2g} and lower e_g orbitals [15]. This imply that the hole possess out of plane d_{3z}^2-r^2 orbital states, while the correcponding number of electrons occupy in plane d_x^2-$_y^2$ orbits. The first-order ZnO Raman spectra involves lattice vibration modes near bloch area, and optical phonons is including $1A_1$, $2B_1$, $1E_1$, and $2E_2$.

The spin polarization transport of double exchange mechanics are observed in LSMO metal insulate

transition, which the substitution of divalent alkaline earth element leads to the mixed valence state of Mn:$Mn^{3+}t_{2g}$ 3d and $Mn^{4+}t_{2g}$ 3d. A temperature driven orbital occupation of diluted d_x^2-$_y^2$ is in the background of crystal field d_{3z}^2-$_r^2$. It is called spin coupling strongly to the lattice. Moreover, the Mn^{3+}-O^{2-}-Mn^{4+} coupling produces ferromagnetic strong correlation through the charge hopping leading to the anomalous magnetization. The vibronic-induced cooperative JT effect blurs the e_g bands and allows the Mn^{3+} e_g electrons to hop into the empty orbital states [10] [11-23].

4. Conclusions

In summary, we have present Raman scattering spectrum on the single and multilayer junction LSMO of orbit-spin couple to the lattice. The spin-orbital dynamics indicated that orbital coupling is origin of lattice anomalies. We emphasize the carrier transport spin-orbit dynamic made by the lattice distortion in ZnO/$La_{0.7}Sr_{0.3}MnO_{3-\sigma}$. The junction resistance properties are adjusted by orbit-spin, magnetic and lattice field. The junction resistance due to field effect and alteration energy band, which are deformed by magnetic structure, crystallographic structure, and carrier concentration. Our measure is attributed to the further understanding of charge order, spin-orbital coupling, magnetic order, optical field and lattice structure and development of photoinduced demagnetization and positive CMR device.

References

[1] R. Vonhelmolt, J. Wecker, K. Samwer, L. Haupt, K. Barner, J. Appl. Phys. **76**, 6925 (1994).

[2] P. Lemmens, G. Guntherodt, C. Gros, Phys. Rep. **375**, 1 (2003).

[3] C. Zener, Phys. Rev. **82**, 403 (1951).

[4] M. F. Cetin, P. Lemmens, V. Gnezdilov, Phys. Rev. B, **85**(19), 195148 (2012).

[5] K. De, S. Das, A. Roy, J. Appl. Phys. **112**(10), 103907 (2012).

[6] V. Gnezdilov, J. Deisenhofer, P. Lemmens, Low Temp. Phys. **38**(5), 419 (2012).

[7] A. Antonakos, E. Liarokapis, G. H. Aydogdu, J. Magnetism and Magnetic Materials, **323**(5), 620 (2011).

[8] R. K. Zheng, Y. Wang, H. L. W. Chan, J. Appl. Phys. **108**(12), 124103 (2010).

[9] A. Ulrich, P. Reto, S. Sverre, Tor Drande, Nicola A. Apaldin, Phys. Rev. B, **88**(8), 054111 (2013).

[10] A. Sawa, T. Fujii, M. Kawasaki, Y. Tokura, Appl. Phys. Lett. **85**, 4073 (2004).

[11] X. P. Zhang, B. T. Xie, Y. S. Xiao, B. Yang et al,

Appl. Phys. Lett., **87**, 072506 (2005).

[12] R. K. Zheng, H. U. Habermeier, H. L. W. Chan, Physical Review B. **81**(10), 104427 (2010).

[13] N. Zhang, T. Geng, H. X. Cao, J. C. Bao, Chin. Phys. B, **17**, 317 (2008).

[14] R. Ren, L. Xuan, W. Weiren, Optoelectron. Adv. Mater.-Rapid Comm., **7**(7-8), 593 (2013).

[15] T. A. Sidorov, Russian J. of Inorganic Chemistry, **58**(6), 8 (2013).

[16] R. Ren, L. Xuan, W. Weiren, J. Appl. Phys. **114**(13), 133705 (2013).

[17] X. Jin, S. Z. Zhao, H. S. Zhang, Clinical EEG and Neuroscience, **42**(1), 53 (2011).

[18] R. Ren, W. Weiren et al, J. Computational Theoretical Nanoscience, **9**(10), 1622 (2012).

[19] R. Ren, W. Weiren, L. Xuan, Physica Scripta. **89**(3), 035601 (2014).

[20] R. Ren, R. Yijing, W. Weiren, Science of Advanced Materials, **6**(6), 1455 (2014).

[21] R. Ren, X. K. Qin, W. Weiren, Rare Metal Materials and Engineering, **42**(1),140 (2013).

[22] X. Jin, H. S. Sheng, J. Clinical Neurophysiology, **29**(3), 230 (2012).

[23] J. R. Sun, Appl. Phys. Lett. **101**(15), 152901 (2012).

_____

*Corresponding author: ren@mail.xjtu.edu.cn,
     rendanan01@126.com